HCNG refuelling station to accelerate the transition towards a real hydrogen economy: A techno-economic analysis

Antonio Sgaramella [*], Lorenzo Mario Pastore, Gianluigi Lo Basso, Ali Mojtahed, Livio de Santoli

Department of Astronautical, Electrical and Energy Engineering, Sapienza University of Rome, Rome, Italy

ABSTRACT

A viable solution for an immediate road transport sector decarbonisation is internal combustion engine vehicles fuelled with H_2 compressed natural gas (HCNG). In this work a techno economic analysis has been carried out in order to optimise the sizing process of a retrofitted HCNG refuelling station with on-site electrolysis, powered by photovoltaic energy. The sizing approach has been addressed by conjecturing a variable hydrogen volumetric fraction in the blend up to 30% vol. Thereafter, once the HCNG effects on the fill-ups demand have been considered, 150 refuelling station capacity scenarios have been analysed by iterating PV plant, electrolyser, and storage systems capacities. Each configuration has been dynamically simulated via a detailed simulation model in the MATLAB/Simulink environment. Hence, by means of the Pareto-based multi-objective optimization and Utopia point the optimal capacity scenarios have been detected by maximising the hydrogen production, and minimising the LCOH, HCNG cost and carbon avoidance cost (CAC) as well. The most suitable HCNG refuelling station ensures an overall H_2 volumetric fraction of 23.98% vol., a LCOH of 9.22 €/kg, 1.18 €/kg as HCNG final cost and carbon avoidance cost of 264.98 €/$tCO_{2,Avd}$.

1. Introduction

Transport sector is crucial in the European economy, contributing around 5% to EU GDP and employing more than 10 million people. At the same time, the transport segment contributes to around 25% of the European's total gas emission, due to its solid reliance on fossil fuels [1–3]. The transport sector decarbonisation is pivotal for the European Climate Law goals achievement of getting to climate neutrality by 2050 [4–6]. Those ambitious targets require a paradigm shift in scoping the issue. Hydrogen (H_2) can play a key role in accomplishing both a clean and prosperous economy [7]. Due to its similar driving range and refuelling time with fossil fuels powered vehicles, the internal combustion engines (ICEs), diesel-powered trains and oil-powered ships replacement with hydrogen fuel cell units is a viable option for the sector greening. Additionally, the hydrogen carrier suits the aviation decarbonisation through synthetic fuels based on H_2, also known as jet fuels [8]. The European Hydrogen Roadmap aims to install 40 GW of electrolysers capacity by 2030 [9]. Accomplishing those ambitious goals requires a remarkable step-up of activities along the whole value chain of each European country. Hydrogen and fuel cell technologies are technically ready for most sectors [10], but the hydrogen economy deployment could fail if insufficient momentum is gained in the transport segment. Coordinated approach by policymakers, industry, and investors is crucial for not leaving fuel cell electric vehicles (FCEVs) and hydrogen refuelling stations (HRS) as a niche solution [11], and for providing economic policy guidelines to develop a solid hydrogen economy not just a business-*as*-usual scenario [12]. HFCEVs and HRS technologies are well proven and ready to step up. Nonetheless, the "chicken-and-egg" problem associated with the priority of either the infrastructures or the end uses still represents a hindrance. Additionally, the lack of adequate policies for zero-emission mobility along with proper fundings are not conductive to significant cost reductions affecting the consumer propensity to encompass the new mobility concept [13,14]. Hydrogen compressed natural gas (HCNG) mixtures can play the role of a bridging technology towards a real transport hydrogen economy [15]. The HCNG strength mostly lies in the refuelling stations, as they do not need to be built from the ground up as the hydrogen refuelling stations do. Indeed, the HCNG refuelling station (RS) can be exploited by upgrading the existing compressed natural gas ones with an additional hydrogen network that envisages the hydrogen

source, the compression and storage systems together with a mixer for the enrichment. The HCNG for retrofitted CNG internal combustion engines is a promising alternative fuel raising ever more attention all over the world. Several studies in literature show significant improvements in brake thermal efficiencies and lower emissions without sacrificing the power output [16–19]. Some modifications regarding fuel injection parameters [20,21] and the cylinder type are needed to run on the hydrogen enriched natural gas fuel, avoiding the tank wall embrittlement. The latter is a topic of considerable discussion regarding the retrofitting of gas pipelines [22]. Furthermore, HCNG is a viable solution for an immediate reduction of CO, CO_2 and NO_X emissions in the transport sector [23]. Thus, customer willingness to convert their habits in aid of hydrogen exploitation for mobility can be stimulated.

2. Literature review and scope of the article

The HRS' sizing process has become one of the main topics related to the hydrogen refuelling infrastructure [24]. Indeed, the hydrogen production and storage capacity along with the cost associated with the hydrogen refuelling stations received a growing attention in the last years [25]. On that purpose Greiner et al. [26] carried out an assessment on the production of hydrogen in Norway for a commuting ferry, including a grid-connected system and an isolated system with wind turbines and a backup power generator. By means of chronological simulations, the main outcomes of that study envisaged hydrogen costs of 6.2 €/kg and 2.8 €/kg for the isolated system and the grid-connected apparatus, respectively. The higher hydrogen costs are due to the larger components' sizes. A techno-economic modelling and analysis of HRS has been carried out in Ref. [27] aiming at outlining the most cost-efficient station design. Here the authors found that the bigger the high-pressure storage banks volume compared to the low-pressure storages, the lower the CAPEX and the OPEX values in the lifespan are. The author proved that the optimal banks number is 4 or maximum 5. Farzaneh-Gord et al. [28] carried out an analysis about the effects of buffer and cascade storage systems on filled mass, filling time, final in-cylinder temperature along with entropy generation in HRS. The buffer storage is the most suitable system in terms of filling time and entropy generation. Bauer et al. [29] analysed the energy behaviour of two different HRSs for fuel cell electric vehicles refuelled at 70 MPa with compressed gaseous and liquid hydrogen. By means of a dynamic simulation the authors estimated 0.37 kWh/kg and 2.43 kWh/kg energy consumptions for the liquid and gaseous stations, respectively. Talpacci et al. [30] evaluated the effect of cascade storage system topology on the cooling energy consumption in HRS. That study demonstrated that the greater the cascade storage system volume, the higher the energy consumption for the cooling is. A techno-economic analysis was carried out by Micena et al. [31] for a solar-powered HRS engineered for a taxi fleet in a Brazilian city. The analysed hydrogen refuelling station comprised an on-site electrolyser fed by the power grid along with a PV system. By changing the taxi fleet supply, the hydrogen costs ranged between 8.96 US$/kg and 13.55 US$/kg. Apostolou et al. [32] investigated the potential of a small-scale autonomous HRS with on-site production via an alkaline electrolyser, powered by a small wind turbine. The sizing process was based on a 6 kg daily hydrogen demand deriving from a fuel cell bicycles fleet. The retail price of the produced hydrogen was estimated to be more than 50.2 €/kg. Thus, in 2017 Reddi et al. [33] carried out an analysis pointing out that the HRS levelized costs for a 200 kg/day dispensing capacity in California were in the range of 6–8 $/kg and 8–9 $/kg for compressed gaseous and liquid hydrogen, respectively. Those costs reached 13–15 $/kg by adding the hydrogen production, packaging and transportation costs. The authors stated that the refuelling station capacity factor affects the final levelized cost up to 40%. Hence, in future FCEV markets the refuelling station's levelized cost can be reduced to 2 $/kg H_2. In Ref. [34] the authors developed an alternative HRS configuration including orifices instead of dispensers as trade-off for safety and economic efficiency. Perna et al. [35] presented a techno-economic analysis of different HRS configurations (450 kg/day) with on-site hydrogen production by means of three different technologies: cracking, autothermal reforming and electrolysis. The main outcomes of that paper show that ammonia-based configurations are the best solutions in terms of overall system efficiency and levelized costs, namely up to 6.89 €/kg. On the other hand, the station with electrolyser technology integrated with the PV system and the national electric grid leads to a levelized hydrogen cost of 7.92 €/kg. Grüger et al. [36] presented a methodology for optimising topology of a wind turbine and electrical grid connected HRS for carsharing vehicles via an evolutionary algorithm. The authors performed their analysis on three different scenarios creating also five different sub-cases by changing the fleet sizes. In Ref. [37] an intelligent operating strategy for electrolysis is proposed aiming at maximising the wind energy generation and fruitfully exploiting the timeslots of low electricity prices. The outcomes of that paper showed that such an intelligent operating strategy benefits the hydrogen production costs by up to 9.2%. In Ref. [38] the authors showed that the most cost-efficient design depends on the grid electricity price, as the higher energy uptake costs make the bigger H_2 production and storage technologies capacities more economically convenient. As pinpointed in this literature review, several research have been carried out on HRS with on-site hydrogen production. Nonetheless, most of the studies involve the energy uptakes also from the grid. In so doing, the sizing approaches are addressed bypassing the RES electrical energy stochasticity.

Numerous progresses in HCNG end-use downstream Power-to-Gas [39] policies applications have been addressed in ICE for transport sector [40], household appliances [41], boilers [42] along with combined heat and power plants [43] and network modelling of integrated energy systems [44]. Notwithstanding, only few research activities address the HCNG refuelling station [45,46], and it is not even deepening the RS sizing process. Thus, the novelty of this paper lies in providing the most adequate sizing approach for a HCNG refuelling stations with on-site green hydrogen production by means of an electrolyser fed by photovoltaic energy. The refuelling station design has been carried out by upgrading an existing CNG refuelling station into a HCNG-RS. Hence, the sizing process has been performed after translating the starter CNG hourly refuelling demand into the blend fill up demand, taking into account the hydrogen effects on the driving ranges and on the overall engine performance. Most of the previous research, that have addressed the HRS sizing process, foresee the energy withdrawal in shunt from the grid and from the PV or wind plants, or from biomass as well. In this study the electrolyser is fed entirely from the PV system. Hence, different technical approaches from the previous studies are accomplished in the adjustment and sizing phase, especially regarding the low-pressure storage system, according to the technical and safety issues. Furthermore, this study aims at providing an innovative sizing approach suitable for determining the HCNG optimal sizes in terms of hydrogen levelized costs along with carbon avoidance costs.

In so doing, the overview of the technical implications and of future energy outlook, deriving from hydrogen exploitation in the mobility sector over the current transition phase, might be valuable for filling the gap in literature dealing with a specific topic like HCNG refuelling stations.

3. Methodology

This assessment copes with how to detect the optimal size of a HCNG refuelling station engineered by upgrading an existing CNG, as depicted in Fig. 1. The case study is located in Rome where a hydrogen branch, including electrolyser, high-pressure storage system (HPSS), low-pressure storage system (LPSS), compressor and mixer device, has been integrated to the CNG system.

The on-site hydrogen production is accomplished by harnessing the PV energy. Therefore, a PV plant has been properly sized in order to achieve hydrogen volumetric fractions in the blend up to 30% vol.
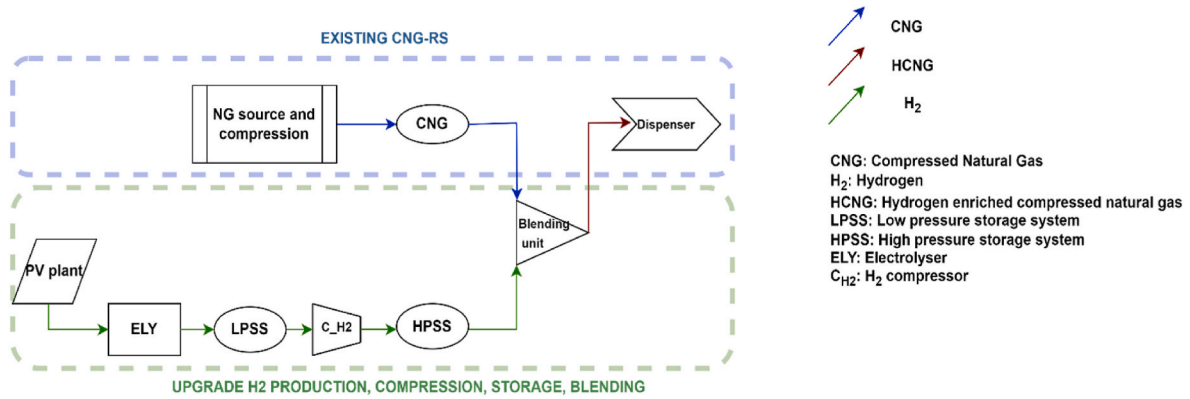
Fig. 1. HCNG refuelling station layout.

Indeed, various tests carried out in previous research showed that 30% vol. in the HCNG benefits the vehicle engines in terms of performance and pollutant emissions [16,23,47]. Yet, the highly varying PV power generation and its entire exploitation for meeting a constant green H_2 demand is not easy to face, especially in winter months. Thus, in order to avoid components oversizing due to the PV stochasticity, a variable H_2 volumetric fraction (*f*) in the blend has been considered, up to 30% vol. In detail, the hydrogen amount for blending is produced by applying to the electrolyser a load-following strategy on PV generation. Several HRS sizing approaches have been widely implemented in the previous studies. Anyway, to the best of the authors knowledge, no assessment dealing with the HCNG refuelling system (RS) sizing has been disclosed yet. In this study a techno economic analysis has been performed in order to optimise the sizing process of a refuelling station with on-site electrolysis, powered by photovoltaic energy. Thus, the initial CNG hourly demand has been translated into 30%vol. hydrogen fraction demand, by considering the hydrogen effect on the driving ranges reduction along with the retrofitted ICE increased efficiencies. Thereafter, once the hourly and daily hydrogen refuelling demands have been

derived, the electrolyser capacity has been identified. Consequently, the initial PV size has been assumed by conjecturing a proportionality factor between the electrolyser and PV plant size. Subsequently, the sizing of the low and high-pressure storage systems has been determined according to the daily hydrogen refuelling demands and the target pressures. Auxiliary components, such as the H_2 compressor, are assumed to be electrically supplied by the PV energy excess and electric grid as well. After setting the first refuelling station scenario, a techno-economic evaluation has been carried out by simulating the yearly HCNG-RS operation in hourly time step via a detailed simulation model in MAT-LAB/Simulink environment. The system comprises alkaline electrolyser, H_2 compressor, LPSS and HPSS sub-models. Additionally, sub-models for refuelling demand, PV energy generation [48] and electricity spot market participation are included in the analysis. Thereafter, 150 configurations have been simulated by ranging PV plant, electrolyser, and the low-pressure storage systems capacities. The HCNG-RS productivity as well as the levelized costs of hydrogen (LCOH), final blends cost and the carbon avoidance values have been calculated. Moreover, a multi-objective optimization process, based on Pareto fronts and Utopia
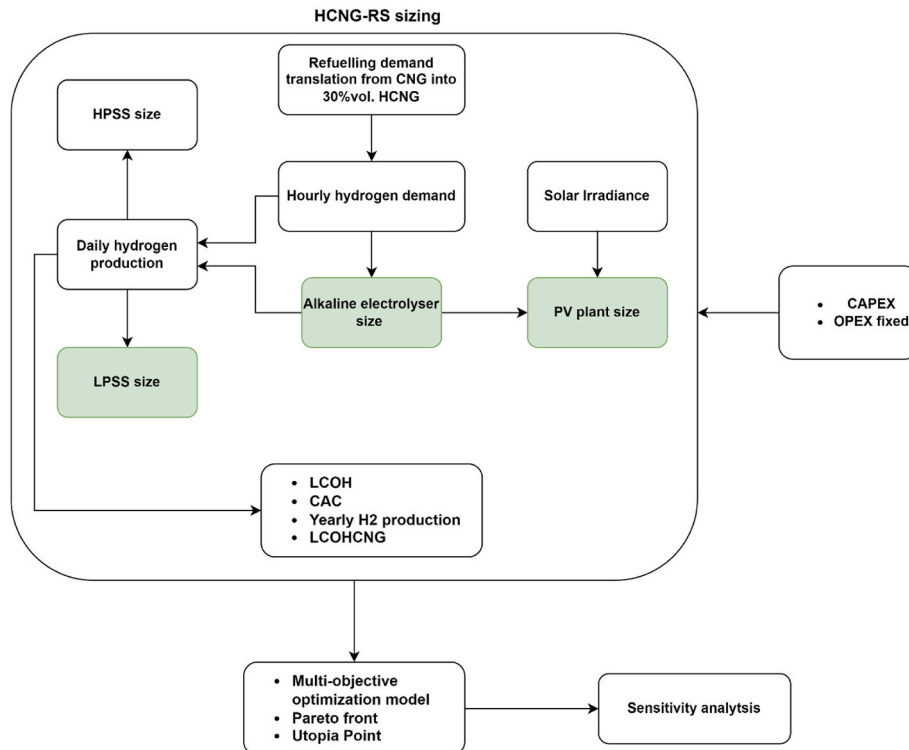

Fig. 2. Main sizing process steps and graphical methodology.

Point, has been carried out aiming at maximising the yearly average H_2 fraction, and minimising the LCOH, HCNG price, the carbon avoidance costs (CAC) and the total installation cost. In the end, a sensitivity analysis on the optimised solutions has been performed by modifying the electrolyser CAPEX.

The logical pathways associated with the applied methodology along with the main steps of sizing process have been graphically outlined in Fig. 2, where the green background subsystems label the iterated components capacities.

3.1. HCNG-RS sizing process

In the next subsections the station dimensioning process has been outlined.

3.1.1. Deriving 30%vol. HCNG refuelling demand

To transpose the share of daily CNG fill-ups into HCNG fuelling demands, the maximum volumetric hydrogen rate per transaction as well as the total transactions number are to be assessed. The upgraded CNG refuelling station records the supply of 2810 kg in a typical day, and up to 3460 kg/day in the peak days. Thus, the effect of the hydrogen fraction in the blend on the driving range and brake specific fuel consumption has been considered in the updated fill-ups transactions. Indeed, as clarified in Table 2, the hydrogen addition in the fuel reduces the driving range up to 21% less, due to the HCNG lessened lower heating value (LHV) and volumetric density compared to CNG. On the other hand, the studies carried out in Refs. [16,23,47,49,50] have found out that the retrofitted internal combustion engines benefit from the hydrogen rate in the blend in terms of brake specific fuel consumption, as reported in Table 1. Hence, the respective HCNG demand has been derived along with the hourly number of maximum fill-ups, as envisaged in Equation (1).

$$M_{30\%HCNG} = M_{CNG} * \frac{E_{CNG}}{E_{30\%HCNG}} * \frac{BTE_{CNG}}{BTE_{30\%HCNG}} \quad (1)$$

Where $M_{30\%HCNG}$ and M_{CNG} stand for the daily mass demand for HCNG with 30% volumetric rate and CNG, respectively [kg/day]. BTE is the brake thermal efficiency [%], and E refers to the pressurised tank energy content [MJ], as described in Equation (2).

$$E = \frac{LHV}{\rho_n} * \rho * V_{tank} \quad (2)$$

Here, LHV is the gaseous fuels lower heating value (MJ/Nm^3), ρ_n is the normal density (kg/Nm^3) and ρ is the volumetric density expressed in kg/m^3. Lastly, V_{tank} is the vehicle tank volume. As the total mass stored in the vehicle cylinder changes according to each blend and the volume of the tank is fixed, the fuels' LHVs have been reported on volumetric basis and not in mass basis, as by definition.

In Ref. [16] Zareei et al. have proved experimentally three different brake thermal efficiency values at 2,000, 4000 and 6000 rpm. For the fill-up conversion the average of the three values has been employed for the CNG and for all the HCNG, as described in Table 1.

In order to meet the customers' refuelling demand, the RS sizing has been engineered to ensure the fill-ups peak demand. A maximum capacity of 10 vehicles per hour per dispenser has been conjectured, by considering 6 min as the overall refuelling duration per customer,

Table 1
Average fuels' brake thermal efficiencies.

Fuel	BTE [%]
CNG	19.53
15%vol. HCNG	22.50
20%vol. HCNG	22.90
25%vol. HCNG	23.02
30%vol. HCNG	23.13

including dispensing and paying time [51,52]. Thereby, the upgraded HCNG refuelling station is equipped with two hoses, similarly to the initial CNG-RS. The resulting daily and hourly HCNG mass dispensed and the hydrogen mass refuelled per each vehicle have been reported in Table 2, by harnessing an average IV type vehicle tank of 0.15 m^3 [28, 45,53].

Table 2 proves that the hydrogen volumetric fractions up to the 20% vol. advantage the driving range. Hence, the fill-ups demand shrinks due to the greater brake thermal efficiencies impact. On the other hand, the hydrogen volumetric fraction (HVF) values ranging between 20%vol. and 30%vol. enhance the refuelling demand because of the stronger impact of the lessened LHV values than the improvements of the increased break thermal efficiencies. Indeed, the higher the volumetric fraction of hydrogen in the blend, the lower the LHV of HCNG. This is because the LHV of H_2 is lower than the LHV of natural gas.

After the upgraded HCNG-RS capacity size has been defined, customer-behaviour information about car refuelling is required. Despite several researchers have conjectured 24 h as HRS daily operation [35,52], the retrofitted HCNG-RS has been sized for 12 h per day, in accordance with the current CNG refuelling station daily working hours. Furthermore, the new hourly mass transactions rate has been derived in accordance with the hourly refuelling transactions outlined by Nexant et al. [51]. Hence, the upgraded HCNG profiles have been built up and depicted in Fig. 3, by distinguishing the Friday peak demand and the average profile over the remaining days [54].

Once the HCNG refuelling station capacity size is defined, the initial sub-models' capacities can be identified.

3.1.2. Electrolyser sizing

The initial alkaline electrolyser capacity has been designed by meeting the Friday peak hydrogen mass flow rate demand. Hence, on the basis of the H_2 peak flow rate, namely 129.895 Nm^3/h, a starting alkaline electrolyser capacity of 689 kW and overall efficiency of 67% (based on LHV) has been assumed [55], taking account that lower loads lead to greater electrolyser efficiencies [56]. Notwithstanding, the electrolyser cannot constantly work at its rated power, due to the stochastic and fluctuating direct PV power supply [57]. Thus, the electrolyser operational strategy consists of running it in load following mode, limiting the partial load to 10% of the rated one, as reported in literature [58–60]. Below this working threshold the oxygen quality is significantly reduced owing to the hydrogen contamination and vice versa, penalising the electrolyser electrical efficiency [61]. Thereby, the hydrogen mass flow rate resulting from fluctuating PV power supply has been computed as described in Equation (3).

$$\dot{m}_{H_2} = P_{ely} * \frac{\eta_{ely}}{LHV_{H_2}} \quad (3)$$

where.

- $\dot{m}_{H_2}$ is the hydrogen mass flow rate (kg/h);
- P_{ely} stands for the incoming electrolyser electrical power (kW);
- η_{ely} denotes the electrolyser efficiency.
- LHV_{H_2} refers to the H_2 lower heating value expressed in kWh/kg.

This electrolyser operational strategy differs from the other research, which foresee to run the on-site electrolysers at narrower partial loads ranges because of additional grid-connected systems [36,37] and back-up power generation sources [26,35]. Those approaches greatly benefit the electrolysis energy efficiency, at the expense of the hydrogen environmental neutrality. Notably, in Refs. [36,37] the authors have addressed the electrolyser working strategy by prioritising the wind farm's energy over a fixed LPSS threshold pressure, and by off-taking energy from the electrical grid at lower LPSS pressures levels. The electrolyser operational strategy is crucial for the green hydrogen production, as significant oversizing is required to cover the peaks of

Table 2
CNG demand upgrade in HCNG demand.

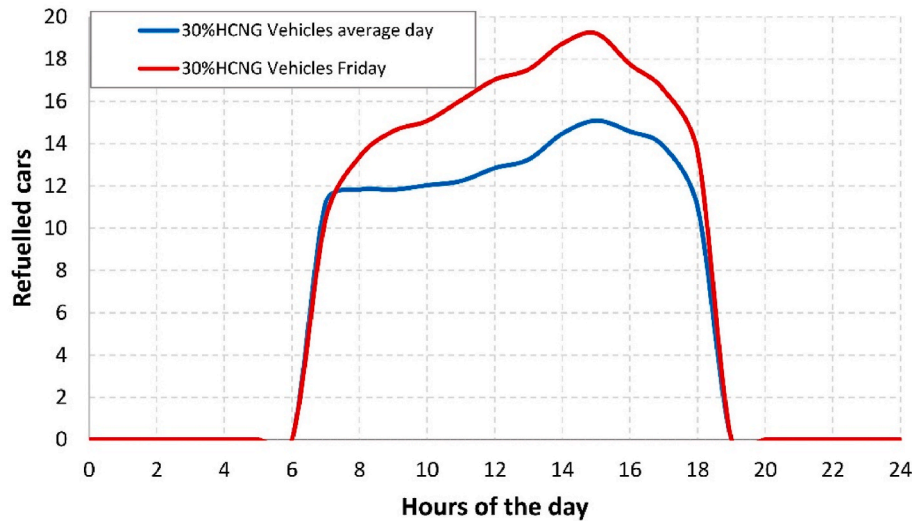| Fuel	LHV [MJ/Nm^3]	ρ_N [kg/Nm^3]	Average/Peak Demand [kg/day]	Average/Peak Fleet [vehicles/day]	Average/Peak Demand [vehicles/hour]
CNG	35.88	0.714	2810/3459.28	144/178	12/15
15%vol. HCNG	32.11	0.62	2366.83/2913.72	140/172	12/14
20%vol. HCNG	30.847	0.589	2300.09/2831.56	143/176	12/15
25%vol. HCNG	29.59	0.558	2258.97/2780.93	148/183	12/15
30%vol. HCNG	28.33	0.527	2216.22/2728.31	154/190	13/16

Fig. 3. 30%vol. HCNG hourly vehicles refuelling demand.

hydrogen demand during overcast days. Hence, this work aims to provide variable HVFs of the blend accordingly with the proper green hydrogen production and storage.

3.1.3. Low-pressure storage system sizing

The low-pressure storage system plays an important role in an optimised HCNG-RS, as it strongly affects the hydrogen production and the specific compression work. Notably, in the specific case of fluctuating hydrogen production, an undersized LPSS leads to a fast vessel emptying at low PV generation, leading to unwanted compressor shutdown and affecting the compressors' lifetime. Moreover, an undersized LPSS can penalise the electrolyser. Indeed, at high PV energy generation a full vessel disables additional hydrogen production, due to lack of capacity. On the other hand, an oversized low-pressure storage volume negatively influences the specific compressor work, due to lower inlet pressure levels. Thus, in this assessment the initial LPSS size has been conjectured equal to the peak daily hydrogen demand and a maximum pressure of 3 MPa, as envisaged in Equation (4) [31,32,36].

$$M_{LPSS} = N_{peak,vehicles} * m_{H_2,vehicle} \tag{4}$$

Here M_{LPSS} stands for the total stored mass in the LPSS buffer, $N_{peak,vehicles}$ refers to the total vehicles refuelled with HCNG on the peak day. Finally, $m_{H_2,vehicle}$ is the total hydrogen mass supplied to the vehicle cylinder filled-up with 30%vol. HCNG. Thereafter, the LPSS volume can be designed.

Hence, the low-pressure storage system function is to operate as a surge buffer [62].

3.1.4. High pressure storage system dimensioning

In order to perform a fast fill-up process meeting the highest hydrogen refuelling demands, the high-pressure storage system (HPSS) is engineered downstream from the hydrogen compressor and upstream from the mixer device. In an upgraded HCNG refuelling station the

maximum HPSS pressure level is 22 MPa. The high-pressure storage tank has been conceived as a buffer during the refuelling process, by ensuring shorter refuelling time. Thereby, with the aim of guaranteeing proper storage capabilities the HPSS has been designed by following the same sizing approach of LPSS and including a safety factor equal to 20%. Equation (5) outlines the designed HPSS stored mass.

$$M_{HPSS} = 1.2 * N_{peak,vehicles} * m_{H_2,vehicle} \tag{5}$$

This sizing approach entails larger stored mass than other studies. Hence, because of the stochastic green hydrogen production, the high-pressure storage system seeks to provide long-term storage capabilities unlike electrical grid supplied electrolysers. Notwithstanding, bigger HPSS capacity allows lower compressor mass flow rate, benefiting the specific H$_2$ compression work along with the compressor CAPEX minimization.

3.1.5. Compressor sizing

Different compression technologies were compared in various studies [63]. The hydrogen compressor type used in this analysis is a reciprocating compressor [64]. Typically, the heat loss associated with reciprocating compressors is 5% or less. Furthermore, in order to reduce the specific compression work, see Equation (6), an air-cooled multi-stage compression system has been considered.

$$W_{sp} = c_p T_{in} \left(\beta^{\frac{k-1}{k} * \frac{1}{\eta_{pol}}} - 1 \right) \tag{6}$$

In Equation (6), β stands for the compression ratio, which is correlated with LPSS state of charge. In order to minimise the specific compressor work, a double stage compressor has been harnessed and the optimised W_{sp} reads as follows:

$$W_{sp} = \sum_{v=1}^{z} c_p T_{in} \left(\beta^{\frac{1}{z}} * \frac{k-1}{k} * \frac{1}{\eta_{pol}} - 1 \right) \tag{7}$$

where.

- $k = \frac{c_p}{c_v}$;
- T_{in}: inlet temperature.
- z stands for the compression stages number.
- η_{pol} is the polytropic efficiency.
- c_p, c_v refer to the specific heat at constant pressure and volume, respectively. These values have been calculated by means of the Langen formula, as shown in Equations (8) and (9) [65].

$$c_p = a + bT \tag{8}$$

$$c_v = (a - R_{H_2}) + bT \tag{9}$$

The hydrogen Langen constant a and b along with R_{H_2} have been described in Table 3.

The compressor mass flow rate is an important parameter for evaluating the capacity and the energy consumption of the compressor, as envisaged in Equations (10) and (11) [31,66,67].

$$P_{comp} = \frac{W_{sp}}{\eta_{comp}} \dot{m}_{comp} \tag{10}$$

$$E_{comp} = \frac{P_{comp}}{\eta_{ele}} * t \tag{11}$$

Here P_{comp} and E_{comp} are the compressor mechanical power and its energy consumption, respectively. $\dot{m}_{comp}$ stands for the outlet compressor mass flow rate, η_{comp} and η_{ele} refer to the compression and electric efficiencies. Lastly, t indicates the compressors working hours.

All the coefficients and values exploited for the compressor sizing and working operation have been outlined in Table 3.

In the simulation the compressor control strategy has been implemented taking into account the LPSS and HPSS states of charge. Basically, when the LPSS stored mass is higher than 9.375 kg and the HPSS is not completely full, the compressor is switched on.

3.2. Economic analysis

The other objective of this work is to determine the optimal HCNG refuelling station sizing by minimising the LCOH and the carbon avoidance cost (CAC) as well. Both values are strongly related to the annual hydrogen supply. Greater H_2 refuelled amount benefits the LCOH and the CAC, expressed in €/kg and €/tCO$_{2,Avd}$, respectively.

Notably, the LCOH is a valuable economic index allowing to evaluate the on-site HCNG-RS competitiveness, by defining the final hydrogen cost [68]. This latter arises from the H_2 production, compression and storage expenditures. Furthermore, engineering, procurement, commissioning (EPC) and site adaptation costs have been included to get the LCOH overarching values [69]. Then, the levelized cost of hydrogen

reads as follows:

$$LCOH = \frac{\sum_{t=1} crf * CAPEX + OPEX - Rev}{M_{H_2}} \tag{12}$$

where.

- LCOH: levelized cost of hydrogen [€/kg$_{H2}$].
- t refers to the single station component.
- crf: capital recovery factor.
- CAPEX: capital expenditure for the component purchase [€].
- OPEX: fixed and variable operation and maintenance costs [€/yr].
- M_{H_2} denotes the yearly hydrogen production [kg].
- Rev refers to the revenues arising from excessive PV energy fed into the grid.

The capital recovery factor (crf) reads as follows [70]:

$$crf = \frac{i * (1 + i)^n}{(1 + i)^n - 1} \tag{13}$$

Here n stands for the technology lifetime and i refers to the nominal discount rate, which has been considered equal to 3%.

After evaluating several literature sources, all cost assumptions have been summarised in Table 4.

The dispenser costs have not been included in the LCOH assessment, because no additional hoses are needed for meeting the updated back-to-back refuelling demand. Hence, the two existing CNG dispensers can be adapted for the blend fill-up with an average HCNG mass flow rate of 0.041 kg/s [45], in accordance with the SAE J2601 safety issues [78–80]. At Ref. [46] the authors carried out a very detailed thermo-dynamic analysis for the HCNG fast and safe refuelling. Thus, the H_2 mass flow rate dispensed by the single nozzle is 7.5 kg/h at most, when the HCNG refuelling at 30%vol. occurs.

Furthermore, the EPC and site adaptation costs have been approximated as 40% of the total CAPEX [36,81]. On the other hand, the PV plant CAPEX already includes the hardware, installation and soft costs [75,82]. The variable OPEX has been determined per each HCNG-RS installation scenario in the simulation process, including energy and water costs [83]. The grid energy purchase and grid sell-back costs are 0.08 €/kWh [84] and 0.052 €/kWh [85], respectively.

Similarly, the blend levelized cost (LCOHCNG) has been computed as reported in Equation (14).

$$LCOHCNG = y_{H_2} LCOH + \left(1 - y_{H_2}\right) C_{CNG} \tag{14}$$

Here, y_{H_2} is the hydrogen mass fraction, see Equation (15), and C_{CNG} stands for the CNG cost, expressed in €/kg$_{CNG}$. The last has been derived from the Italian station CNG price [86].

Table 3
Data for compressor sizing.

Parameters	Value	Ref.
T_{in} [K]	288	Assumed
η_{pol} [%]	91	[35,64]
a [kJ/kgK]	13.8	[65]
b [kJ/kgK^2]	0.00222	[65]
R_{H_2} [kJ/kgK]	4.157	Calculated
η_{comp} [%]	70	[31,66]
η_{ele} [%]	90	[30,67]
$\dot{m}_{comp}$ [kg/h]	9.375	Calculated

Table 4
Cost assumptions.

Component	CAPEX	OPEX	Life span	Source
Electrolyser	1327 €/kW	2%[a]CAPEX	80,000 h	[26,36,69]
H$_2$ Storage (3 MPa)	600 €/kg	5 €/kg/yr	20 years	[36,71]
H$_2$ storage (22 MPa)	773.5 €/kg	8 €/kg/yr	20 years	[27,72]
Compressor	4500 €/kW	8%[a]CAPEX	20 years	[27,35,73,74]
PV plant	1000 €/kW	15.4 €/kW/yr	20 years	[75,76]
Mixer	13,302.378$y^{-0.613a}$	0	20 years	[77]

[a] y refers to the H$_2$ Nm^3/h flow rate.

$$y_i = f_i \frac{MW_i}{MW_{blend}} \tag{15}$$

In Equation (15) f_i refers to the component volumetric fraction, MW_i and MW_{blend} are the single component and blend molecular weight, respectively.

3.3. Environmental analysis

The potential transport sector greening, hailing from the retrofitted internal combustion engines fuelled with HCNG, has been evaluated via a specific indicator. In detail, the CO_2 avoided emissions ($CO_{2,Avd}$) [87] have been calculated for each HCNG-RS scenario.

The yearly avoided natural gas mass (NG_{Avd}) originated from the total HCNG fill-ups reads as follows:

$$NG_{Avd} = 365 * (m_{tank,100\%CNG} * N_{average,CNGvehicles} - y_{CNG}m_{tank,HCNG}$$
$$* N_{average,HCNGvehicles}) \tag{16}$$

In Equation (16) $m_{tank,100\%CNG}$ is the total fillable CNG mass in the not retrofitted tank, $N_{average,CNGvehicles}$ refers to the daily average CNG refilled vehicles and y_{CNG} stands for the average CNG mass fraction in the average blend. Similarly, $m_{tank,HCNG}$ is the total HCNG mass tank and $N_{average,HCNGvehicles}$ is the average daily HCNG refuelled vehicles.

Hence, the resulting yearly CO_2 avoided ($CO'_{2,Avd}$), derived by the natural gas replacement with green hydrogen has been computed by Equation (17).

$$CO'_{2,Avd} = \frac{NG_{Avd}}{\rho_{n,NG}} LHV_{NG} f_{em,NG} \tag{17}$$

Here, $\rho_{n,NG}$, LHV_{NG} and $f_{em,NG}$ refer to the normal NG density, lower heating value and CO_2 emission factor. This latter is equal to 55.954 tCO_2/TJ [88].

Notwithstanding, $CO'_{2,Avd}$ does not include the CO_2 emissions accounted from the grid electrical energy exploited by the H_2 compressor ($E_{el,grid}$). Therefore, by considering the Italian grid CO_2 emission factor ($f_{em,grid}$) equal to 260.5 gCO_2/kWh [89], the overall CO_2 avoided ($CO_{2,Avd}$) has been computed by Equation (18):

$$CO_{2,Avd} = CO'_{2,Avd} - E_{el,grid} * f_{em,grid} \tag{18}$$

finally, the carbon avoidance cost can be evaluated according to the following equation:

$$CAC = \frac{LCOH * M_{H_2} - LCONG * NG_{Avd}}{CO_{2,Avd}} \tag{19}$$

where M_{H_2} is the yearly refuelled hydrogen mass.

Table 5 summarises all the applied data for the environmental analysis.

3.4. Multi-objective optimization model

In this study the most environmentally sustainable and economically competitive HCNG-RS layouts have been detected by means of a Pareto-based multi-objective optimal criterium [7]. This approach allows to identify the optimal PV plant, electrolyser and LPSS capacities that enhance the overall system efficiency benefitting the customers' satisfaction. The multi-objective approach [91] has been mathematically addressed as in Equation (20), in accordance with Ref [92–94].

minimise: $y = F(x) = (F_1(x), F_2(x), ..., F_k(x))$.
subject to: $g(x) = (g_1(x), g_2(x), ..., g_m(x)) \leqslant 0$.

$$h(x) = (h_1(x), h_2(x), ..., h_p(x)) = 0 \tag{20}$$

$l_i \leqslant x_i \leqslant u_i, i = 1, 2, ..., n$

where: $x = (x_1, x_2, ..., x_n) \in X$.

$y = (y_1, y_2, ..., y_k) \in Y$

Here x refers to the iterated values of the n decision variable. These parameters are listed into a range bounded by lower and upper limits, defined as l_i and u_i, respectively, in a decision space X. The overall vector of k objective functions is associated to y and it is a member of the objective space, denoted with Y. Moreover, $g(x)$ represents a set of inequality constraints with feasible solutions. $h(x)$ indicates the set of p equality constraints. The decision variables of optimization and their ranging values have been listed in Table 6. Thereby, 150 HCNG-RS capacities have been analysed and all the x values, meeting Equation (20) requirements, create feasible solutions set, where some x Pareto solutions dominate other candidate parameters x'. Such dominance rule is regulated as follows [7]:

$$\begin{cases} F_i(x) \leq F_i(x'), \forall i \in \{1, 2, \cdots, m\} \\ F_i(x) < F_i(x'), \exists i \in \{1, 2, \cdots, m\} \end{cases} \tag{21}$$

The not dominated Pareto solutions outline the Pareto front. Each Pareto scenario represents a solution that cannot be improved in one of the objectives without negatively affecting another objective.

Finally, the optimal RS capacities have been identified via the mathematical expedient of the Utopia point (UP). The UP represents an ideal but unfeasible solution, that meets the best requirements for a scenario. Particularly, considering a two-objective minimization problem, the Utopia point is a point whose abscissa is associated to the best value accounted on the y-axis and as ordinate the best value presented on the x-axis. Hence, the optimal scenarios are easily identifiable as the solutions characterised by the minimal distance from the UP, as shown in the following equations [93,95].

$$\min(P_{solution}) \tag{22}$$

$$P_{solution} = \sqrt{\sum_j (F_{jUtopia} - F_j)^2} \tag{23}$$

Here, $P_{solution}$ stands for the distance between the normalised objective j function and the detected UP; $F_{jUtopia}$ is the allowed minimum value of normalised objective function j. Lastly, F_j is the non-minimum possible value of normalised objective function j.

The scenarios delineated by the Utopia Point represent the potential optimal scenarios for the total CAPEX, LCOH, LCOHCNG and CAC minimisation along with the total yearly refuelled hydrogen maximisation.

Table 5
Italian grid emissions parameters.

Parameters	Value	Ref.
%RES$_{grid}$	36%	[87]
f_c	0.914	[87]
$\eta_{thel,grid}$	0.422	[90]
$f_{nr,el\ grid}$	1.571	Calculated
$f_{ren,el\ grid}$	0.394	Calculated
$f_{em,NG}$ [tCO_2/TJ]	55.954	[88]
$f_{em,grid}$ [gCO_2/kWh]	260.5	[89]

Table 6
Decision variables of optimization.

Decision variable	Range	Step size
PV plant rate power [kW]	2400–1400	200
Electrolyser's rated power [kW]	827–552	69
LPSS stored mass [kg]	154–98	14

4. Results and discussion

In this section, the outcomes of this analysis have been presented and discussed. At first, the yearly HCNG-RS simulation has been carried out in MATLAB/Simulink environment with the conjectured subsystem sizes, comprising electrolyser capacity of 689 kW, 2000 kW PV plant and 139 kg of H_2 in the LPSS with a CAPEX of 3.29 M€. Thereby, an average yearly H_2 volumetric rate of 23.455% has been computed, resulting in the LCOH and LCOHCNG values of 10.02 €/kg_{H2} and 1.18 €/kg_{HCNG}, respectively. Moreover, the CAC value arising from these capacities is 302.06 €/$t_{CO2,Avd}$. In light of these values, other electrolysers, PV plants and LPSS combinations have been simulated, in order to optimise the overall system efficiency. The outcomes have been presented in the following subsections.

4.1. Optimal HCNG refuelling station capacities

As mentioned above, the most suitable HCNG refuelling station size, that addresses both economic and environmental purposes, cannot be sought just optimising one single parameter among the average yearly volumetric fraction, LCOH, LCOHCNG, CAC and total investment costs. Therefore, three regions of feasible solutions have been set, in order to clearly detect the non-dominated Pareto solutions, by exploiting the corresponding Pareto front. Figs. 4–6 provide the different placements of the feasible subsystem combinations in accordance with the optimised parameters. In Figs. 4–6 all the RS configurations have been represented by dots, coloured according to a cost scale. The light blue indicates the lowest investment costs. On the other hand, the red scenarios record the highest CAPEX values, owed to the greater PV and electrolyser capacities. Fig. 4 shows the 150 eligible capacity scenarios arranged according to the simultaneous LCOH minimization and HCNG hydrogen volumetric fraction maximisation.

From the LCOH minimization point of view, the higher the yearly hydrogen production the lower the LCOH is. Notwithstanding, in this analysis the hydrogen is produced by exploiting the stochastic PV energy only, and a wider PV and electrolyser capacities range has been investigated in order to find the trade-off between overall system efficiency and economic profitability. In this phase, the incomes deriving from the renewable energy excess sell-back have not been considered in the LCOH analysis, ensuring optimal PV-electrolyser capacities combinations. The LPSS affects the overall system efficiency and consequently the LCOH as well. Indeed, the low-pressure storage system not merely operates as a surge buffer, but it strongly impacts the compressor work as well. Despite greater hydrogen production lessening the LCOH values, higher average HVF leads to higher LCOHCNG values, due to the higher hydrogen costs than CNG. Thereby, the red dots record the highest
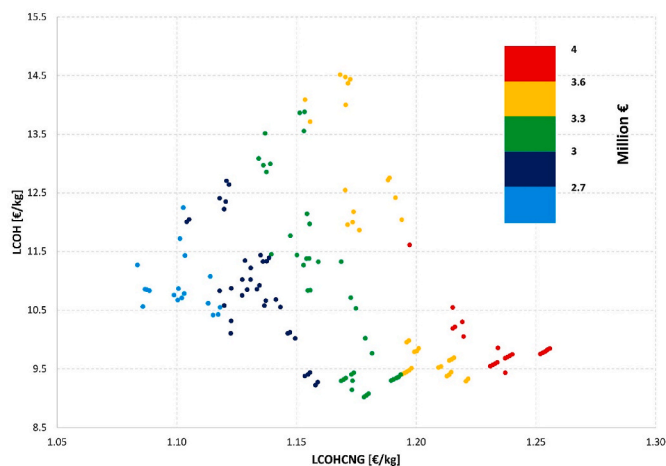
Fig. 5. Region of eligible sizing combination, LCOH-LCOHCNG Pareto front.

levelized costs of the blend, due to the greater on-site green H_2 production. Fig. 5 depicts the PV-electrolyser-LPSS installation scenario combinations arranged in accordance with the respective LCOH and LCOHCNG values.

Fig. 6 shows the feasible HCNG-RS sizes settled according to the LCOH and CAC minimization. Specifically, lower LCOH values benefit the final CAC, in accordance with Equation (21). The blends' average hydrogen fraction strongly affects the CAC. Indeed, the greater the hydrogen volumetric concentration, the lower the LCOH, the LHV and the density are (see Table 2), and the higher the avoided natural gas is. In the current analysis the daily refuelled vehicle number is kept constant per each resulting hydrogen fractions, as those latter occur at the 30%vol. HCNG fill-up number. Notwithstanding, as the overall driving range increases at lower blend hydrogen fractions, the daily refuelling demand shrinks, affecting the NG_{Avd}. The CNG-30%vol. HCNG driving range parity can be achieved by enhancing the vehicle tank pressure up to 15% more, having fixed its volume. Similarly, the same driving range can be attained at equal tank pressure, by expanding the cylinder volume of 7% more.

The Pareto Fronts of Figs. 4–6 provide different optimal solutions in accordance with the respective optimization parameters. The most suitable HCNG refuelling station installation capacities have been computed via the Utopia Point detection, by assigning equal weight to the profitability and to the environmental sustainability. The five optimal PV, electrolyser and LPSS capacity scenarios are shown in Table 7.

The presented outcomes, arising from this specific case study, reveal that the 10% electrolyser oversizing in combination with the 20% PV under-sizing is the most economic and environmental effective solution. Indeed, despite the optimal scenario envisages a slight increase of green H_2 production compared to the first HCNG size, it ensures the 8% LCOH saving, along with 12.27% CAC reduction. Thereafter the computed optimal HCNG-RS size encompasses significant yearly CO_2 and NG savings, amounting to 545.43 tonnes and 200.783 tonnes, respectively.

These environmental and economical upgrades are derived by coupling the electrolyser and the PV plant by applying a capacity ratio equal to 1/2.11. In the assessment carried out in Ref. [96] the authors found out that the optimal electrolyser capacity for an HRS is equal to 57.7% of the dedicated PV plant capacity installed in Vietnam. Therefore, this assessment proves that for a variable hydrogen production, the most suitable electrolyser capacity is the 47.4% of the dedicated PV plant installed in Rome.

The multi-objective optimization analysis for the optimal HCNG system capacities has been carried out not accounting for the electricity spot market, in order to perform a more accurate optimization and avoiding a strong LCOH minimization affection by the electricity sell-
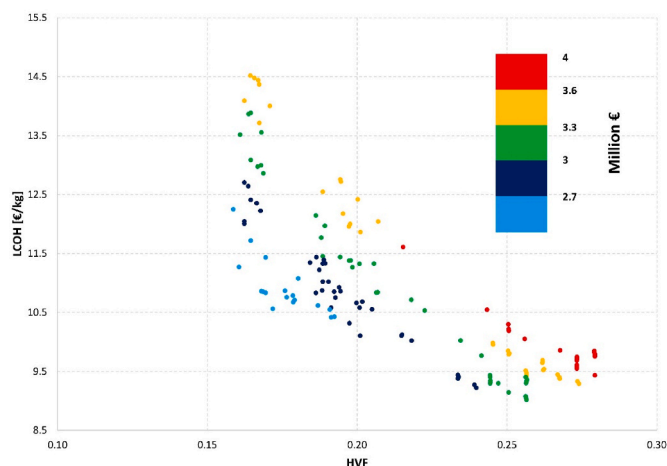

Fig. 4. Region of eligible sizing combination, LCOH-H_2 Pareto front.
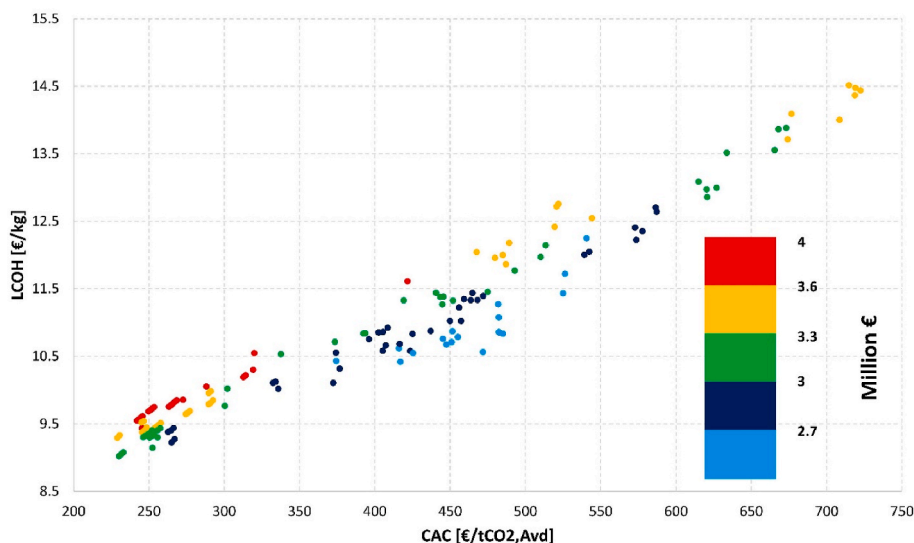
Fig. 6. Region of eligible sizing combination, LCOH-CAC Pareto front.

Table 7
Optimal HCNG-RS capacities.

Value	$P_{solution}$ [/]	LCOH [€/kg]	H_2 volumetric fraction [%]	LCOHCNG [€/kg]	CAC [€/t_{CO2}]	CAPEX [M€]	PV, Electrolyser, LPSS [kW, kW, kg]
U P	/	9.020	27.93	1.083	228.992	2.48	/
#1	0.2493	9.222	23.98	1.181	264.98	2.98	1600, 759, 139
#2	0.2524	9.379	23.36	1.172	262.74	2.96	1600, 759, 98
#3	0.2545	9.274	23.91	1.182	267.05	2.99	1600, 759, 154
#4	0.2559	9.404	23.38	1.174	264.78	2.965	1600, 759, 112
#5	0.2598	9.438	23.36	1.175	266.38	2.97	1600, 759, 126

back revenues. Nonetheless, the electricity spot market impact has been then evaluated in the LCOH, LCOHCNG and CAC computation for the detected optimal capacities, as shown in Fig. 7. All the scenarios benefit from a LCOH reduction, ranging between 7% and 9%. Similarly, the sold PV energy to the grid affects the LCOHCNG, accounting for a reduction of 4% of costs. Lastly, significant CAC decreases occur up to 19%, proving the strong LCOH impact on the carbon avoidance costs.

4.2. Sensitivity analysis

The previous analysis has proved the LCOH effect on the LCOHCNG and CAC. Thereby, considering the significant electrolyser impact on the CAPEX system, a sensitivity analysis, by changing that parameter, has been performed to evaluate the potential LCOH variation. Electrolysers' costs reduction along with longer lifetimes and higher efficiencies can

open a new development in the hydrogen economy allowing the electrolysers quality leap, by moving from niche technologies to mainstream technologies. Fig. 8 shows the optimised LCOH values resulting from electrolysers' CAPEX variation in a range of 900–1700 €/kW.

This figure points out that the electrolyser's CAPEX lessening to 900 €/kW leads to a LCOH reduction up to 13.6%; on the other hand, at 1700 €/kW the LCOH increases up to 11.9%. Fig. 7 reveals that the lowest LCOH value is not recorded at the highest or the lowest LPSS capacity. Indeed, those capacities allow greater H_2 production or lower CAPEX values, respectively. The lowest LCOH value at the fixed PV and electrolyser capacities is provided by the LPSS capacity that benefits the global system efficiency, optimising the compressor work and the energy off-take. The greater the compressor sizes the more impactful the storage system capacity is.

Moreover, due to the greater *f*, the final LCOHCNG values of the lowest LCOH scenarios are the least economically competitive, see Fig. 9.

Fig. 10 proves that scenarios with the lowest LPSS capacities benefit from a lower CAC, owed to the reduced compressor work and energy off-take. In Fig. 11 the LCOH lessening is emphasised, by the comparison between the initial scenario and the detected optimal scenario.

The main aspect that preponderantly emerges from Fig. 10 is the significative CAPEX footprint on the final LCOH. The EPC and site adaptation costs impact the LCOH up to 12% in the optimal HCNG-RS size. Lastly, the variable and fixed OPEX costs account for only the 18% on the final LCOH. Per each HCNG refuelling station size the CAPEX weight on the LCOH arises up to 70%. Notably, for this HCNG RS the 90% of the total costs is associated to the green hydrogen production and just the 10% to the H_2 compression, storage and blending at 22 MPa, as depicted in Fig. 12.

Particularly, in the best detected scenario the 61% of the green H_2 production cost is attributed to the PV plant and the remaining 39% is
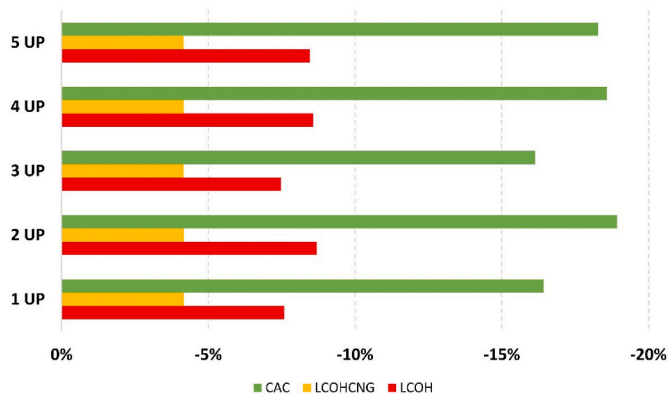
Fig. 7. Electricity spot market impact on LCOH, LCOHCNG, CAC.
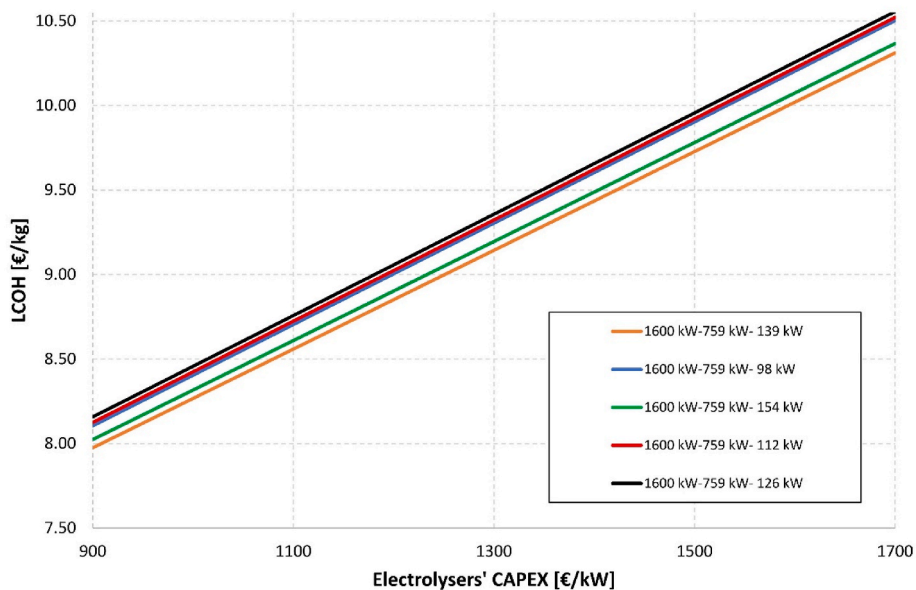
Fig. 8. LCOH variation vs. electrolyser CAPEX.
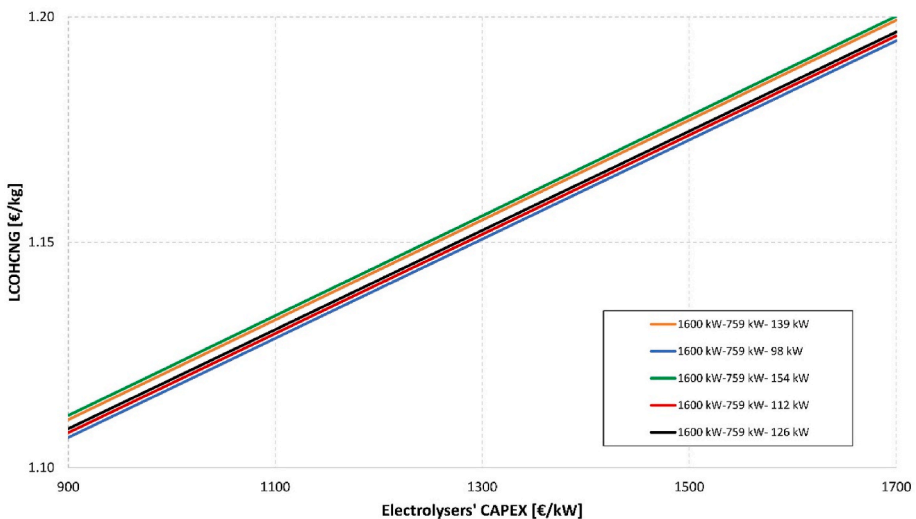
Fig. 9. LCOHCNG variation vs. electrolyser CAPEX.

owed to the electrolyser technology.

A further LCOH lessening can be recorded by considering the electricity spot market. Hence, the optimal capacity scenario LCOH can be decreased up to 8.52 €/kg and 7.28 €/kg by reducing the electrolyser's CAPEX from 1327 €/kW to 900 €/kW.

5. Conclusion

In this work a techno economic analysis has been carried out in order to optimise the sizing process of a retrofitted HCNG refuelling station with on-site electrolysis, powered by photovoltaic energy only. In detail, the hydrogen amount for blending is produced by applying to the electrolyser a load-following strategy on PV generation. Hence, a variable HVF in the blend has been considered up to 30%, in order to mitigate components oversizing due to the PV stochasticity. Thereafter, once the HCNG effects on the fill-ups demand have been considered, 150 RS capacity scenarios have been analysed with iterating PV plant, electrolyser, and storage systems capacities. Each configuration has been dynamically simulated in hourly time steps via a detailed

simulation model in the MATLAB/Simulink environment. Thus, by means of the Pareto-based multi-objective optimal criterium and Utopia point the optimal capacity scenarios have been detected by maximising the hydrogen production, and minimising the LCOH, LCOHCNG and CAC as well.

The main outcomes of this paper can be summarised as follows.

- The HCNG refuelling station can be engineered as a CNG-RS upgrade.
- Hydrogen volumetric fractions up to the 20%vol. benefit the driving range, shrinking the fill-ups demand due to the greater break thermal efficiencies impact. On the other hand, the volumetric H_2 rates ranging between 20%vol. and 30%vol. enhance the refuelling demand because of their more reduced LHV.
- The CNG-30%vol. HCNG driving range parity can be achieved by enhancing the stored vehicle tank pressure up to 15% at fixed volume. Similarly, at same tank pressure, the driving range equality can be accomplished by expanding the vehicle cylinder volume up to 7%.
- The greater the hydrogen rate the lower the LCOH is and the greater the LCOHCNG is.
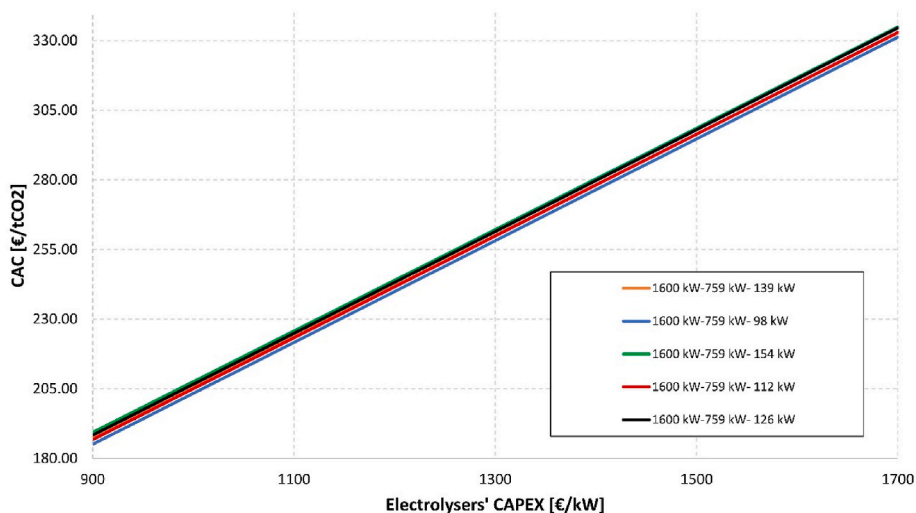
Fig. 10. CAC variation vs. electrolyser CAPEX.
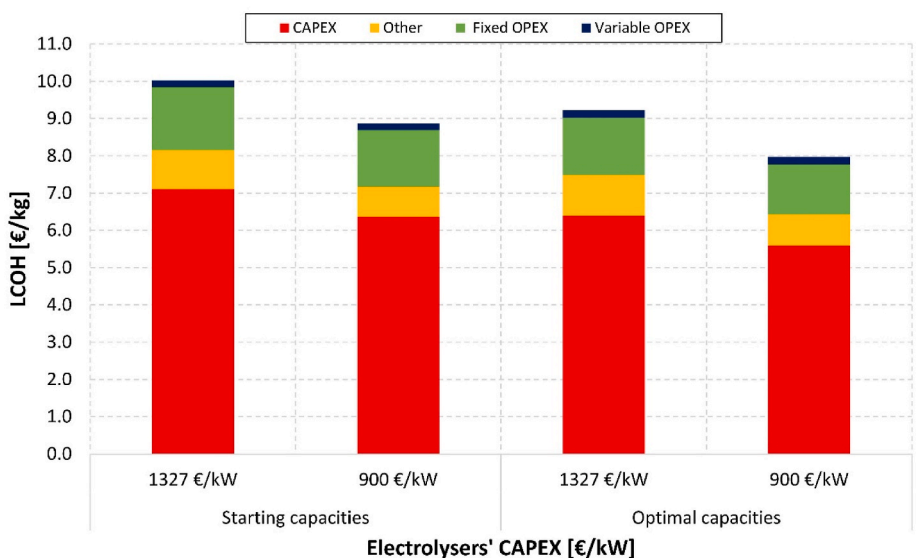
Fig. 11. LCOH breakdown in cost.
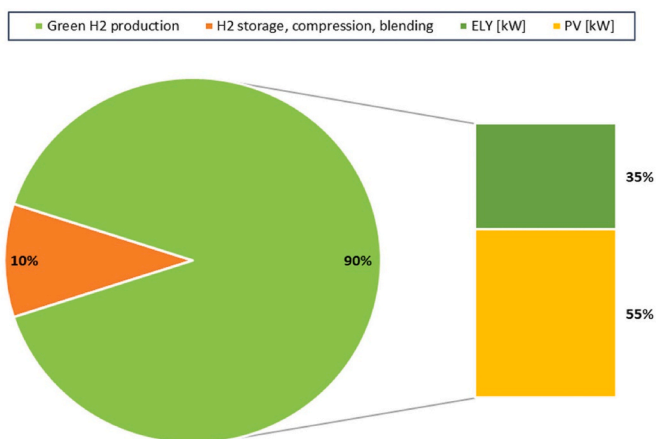
Fig. 12. HCNG-RS CAPEX breakdown.

● The 10% electrolyser oversizing in combination with the 20% PV under-sizing is the most economic and environmental effective solution.

● The optimal scenario detected via Utopia point comprises the 1/2.11 electrolyser-PV capacity ratio and ensures a yearly average blend of 23.98%vol. The optimised capacities disclose a CO_2 and NG savings, amounting to 545.43 tonnes and 200.78 tonnes, respectively.

● The electricity spot market incomes lessen the LCOH values up to 9%. Thereby, CAC and LCOHCNG are diminished by 19% and 4%, respectively.

● The HCNG-RS CAPEX affects the LCOH value up to 70%. As a consequence, by reducing the electrolyser CAPEX to 900 €/kW and considering the hot spot market incomes, the LCOH value lessens to 7.28 €/kg.

● The 90% of the total costs is associated with the green hydrogen production and just the 10% to the H_2 compression, storage and blending at 22 MPa.

As a side conclusion, the results and the envisaged approach in this article foresee to provide a practical tool useful for private companies, in order to ensure the cost effectiveness and their investments profitability.

In this regard, a possible further development of this work could include an economic analysis that incorporates the return on common equity of the HCNG RS, including the land costs for the PV plant construction.

Nomenclature

CAC	Carbon Avoidance Cost
CAPEX	Capital expenditure
CNG	Compressed natural gas
CNG-RS	Compressed natural gas refuelling station
$CO_{2,Avd}$	Avoided Carbon dioxide
crf	Capital recovery factor
f	Hydrogen volumetric fraction
FCEV	Fuel cell electric vehicles
H_2	Hydrogen
HCNG	Hydrogen compressed natural gas
HCNG-RS	HCNG refuelling station
HPSS	High pressure storage system
HRS	Hydrogen refuelling station
HVF	Hydrogen volumetric fraction
ICE	Internal combustion engine
LCOH	Levelized cost of hydrogen
LCOHCNG	Levelized cost of HCNG
LHV	Lower heating value
LPSS	Lower pressure storage system
NG	Natural gas
NG_{Avd}	Avoided natural gas
OPEX	Operational expenditure
PV	Photovoltaic
RS	Refuelling station
UP	Utopia Point

CRediT authorship contribution statement

Antonio Sgaramella: Writing – original draft, Software, Resources, Project administration, Methodology, Investigation, Formal analysis, Data curation, Conceptualization. **Lorenzo Mario Pastore:** Conceptualization. **Gianluigi Lo Basso:** Writing – review & editing, Supervision. **Ali Mojtahed:** Writing – review & editing. **Livio de Santoli:** Supervision.

Declaration of competing interest

The authors declare that they have no known competing financial interests or personal relationships that could have appeared to influence the work reported in this paper.

References

[1] European Commision. Transport and the green deal n.d. https://commission.eur opa.eu/strategy-and-policy/priorities-2019-2024/european-green-deal/transpor t-and-green-deal_en. [Accessed 23 March 2023].

[2] IEA. Improving the sustainability of passenger and freight transport n.d. https://www.iea.org/topics/transport. [Accessed 23 March 2023].

[3] European Environment Agency. Air pollution sources n.d. https://www.eea.europ a.eu/themes/air/air-pollution-sources-1 (accessed March 23, 2023).

[4] Eprs. Reducing methane emissions in the energy sector. n.d.

[5] Pastore LM, Lo Basso G, Cristiani L, de Santoli L. Rising targets to 55% GHG emissions reduction – the smart energy systems approach for improving the Italian energy strategy. Energy 2022;259. https://doi.org/10.1016/j. energy.2022.125049.

[6] EU economy and society to meet climate ambitions. European Green Deal: commission proposes transformation of EU economy and society to meet climate ambitions n.d. https://ec.europa.eu/commission/presscorner/detail/%5Beuropa_t okens:europa_interface_language%5D/ip_21_3541. [Accessed 23 March 2023].

[7] Sgaramella A, Pastore LM, Lo Basso G, de Santoli L. Optimal RES integration for matching the Italian hydrogen strategy requirements. Renew Energy 2023;219. https://doi.org/10.1016/j.renene.2023.119409.

[8] Zhang C, Hui X, Lin Y, Sung CJ. Recent development in studies of alternative jet fuel combustion: progress, challenges, and opportunities. Renew Sustain Energy Rev 2016;54:120–38. https://doi.org/10.1016/j.rser.2015.09.056.

[9] van Wijk Jorgo Chatzimarkakis A. Green hydrogen for a European green deal A 2x40 GW initiative. n.d.

[10] Kovač A. Hydrogen and fuel cells: preface to the special issue on the 14TH conference on sustainable development of energy, water, and environment systems (SDEWES2019). Int J Hydrogen Energy 2021;46:10015. https://doi.org/10.1016/ j.ijhydene.2021.01.029.

[11] Westend. A SUSTAINABLE PATHWAY FOR THE EUROPEAN ENERGY TRANSITION HYDROGEN ROADMAP EUROPE n.d. https://doi.org/10.28 43/249013.

[12] Kovač A, Paranos M, Marciuš D. Hydrogen in energy transition: a review. Int J Hydrogen Energy 2021;46:10016–35. https://doi.org/10.1016/j. ijhydene.2020.11.256.

[13] Yan J, Zhao J. Willingness to pay for heavy-duty hydrogen fuel cell trucks and factors affecting the purchase choices in China. Int J Hydrogen Energy 2022;47: 24619–34. https://doi.org/10.1016/j.ijhydene.2022.03.252.

[14] Kim JH, Kim HJ, Yoo SH. Willingness to pay for fuel-cell electric vehicles in South Korea. Energy 2019;174:497–502. https://doi.org/10.1016/j.energy.2019.02.185.

[15] Nastasi B, Lo Basso G. Hydrogen to link heat and electricity in the transition towards future Smart Energy Systems. Energy 2016;110:5–22. https://doi.org/ 10.1016/j.energy.2016.03.097.

[16] Zareei J, Rohani A, Mazari F, Mikkhailova MV. Numerical investigation of the effect of two-step injection (direct and port injection) of hydrogen blending and natural gas on engine performance and exhaust gas emissions. Energy 2021;231. https://doi.org/10.1016/j.energy.2021.120957.

[17] Deng J, Ma F, Li S, He Y, Wang M, Jiang L, et al. Experimental study on combustion and emission characteristics of a hydrogen-enriched compressed natural gas engine under idling condition. Int J Hydrogen Energy 2011;36:13150–7. https://doi.org/ 10.1016/j.ijhydene.2011.07.036.

[18] Khandal SV, Banapurmath NR, Gaitonde VN. Effect of hydrogen fuel flow rate, fuel injection timing and exhaust gas recirculation on the performance of dual fuel engine powered with renewable fuels. Renew Energy 2018;126:79–94. https://doi. org/10.1016/j.renene.2018.01.049.

[19] Bauer CG, Forest TW. EEect of hydrogen addition on the performance of methane-fueled vehicles. Part II: driving cycle simulations 2001;26.

[20] Mathai R, Malhotra RK, Subramanian KA, Das LM. Comparative evaluation of performance, emission, lubricant and deposit characteristics of spark ignition engine fueled with CNG and 18% hydrogen-CNG. Int J Hydrogen Energy 2012;37: 6893–900. https://doi.org/10.1016/j.ijhydene.2012.01.083.

[21] Bysveen M. Engine characteristics of emissions and performance using mixtures of natural gas and hydrogen. Energy 2007;32:482–9. https://doi.org/10.1016/j. energy.2006.07.032.

[22] Qiu Y, Zhou S, Gu W, Ding S, Han G, Zhang K, et al. Multi-stage flexible planning of regional electricity-HCNG-integrated energy system considering gas pipeline retrofit and expansion. IET Renew Power Gener 2022;16:3339–67. https://doi. org/10.1049/rpg2.12586.

[23] Zareei J, Rohani A, Wan Mahmood WMF. Simulation of a hydrogen/natural gas engine and modelling of engine operating parameters. Int J Hydrogen Energy 2018;43:11639–51. https://doi.org/10.1016/j.ijhydene.2018.02.047.

[24] Minutillo M, Perna A, Di Trolio P, Di Micco S, Jannelli E. Techno-economics of novel refueling stations based on ammonia-to-hydrogen route and SOFC technology. Int J Hydrogen Energy 2021;46:10059–71. https://doi.org/10.1016/j. ijhydene.2020.03.113.

[25] Šimunović J, Pivac I, Barbir F. Techno-economic assessment of hydrogen refueling station: a case study in Croatia. Int J Hydrogen Energy 2022;47:24155–68. https:// doi.org/10.1016/j.ijhydene.2022.05.278.

[26] Greiner CJ, KorpÅs M, Holen AT. A Norwegian case study on the production of hydrogen from wind power. Int J Hydrogen Energy 2007;32:1500–7. https://doi. org/10.1016/j.ijhydene.2006.10.030.

[27] Blazquez-Diaz C. Techno-economic modelling and analysis of hydrogen fuelling stations. Int J Hydrogen Energy 2019;44:495–510. https://doi.org/10.1016/j. ijhydene.2018.11.001.

[28] Farzaneh-Gord M, Deymi-Dashtebayaz M, Rahbari HR, Niazmand H. Effects of storage types and conditions on compressed hydrogen fuelling stations performance. Int J Hydrogen Energy 2012;37:3500–9. https://doi.org/10.1016/j. ijhydene.2011.11.017.

[29] Bauer A, Mayer T, Semmel M, Guerrero Morales MA, Wind J. Energetic evaluation of hydrogen refueling stations with liquid or gaseous stored hydrogen. Int J Hydrogen Energy 2019;44:6795–812. https://doi.org/10.1016/j. ijhydene.2019.01.087.

[30] Talpacci E, Reuß M, Grube T, Cilibrizzi P, Gunnella R, Robinius M, et al. Effect of cascade storage system topology on the cooling energy consumption in fueling stations for hydrogen vehicles. Int J Hydrogen Energy 2018;43:6256–65. https:// doi.org/10.1016/j.ijhydene.2018.02.030.

[31] Micena RP, Llerena-Pizarro OR, de Souza TM, Silveira JL. Solar-powered hydrogen refueling stations: a techno-economic analysis. Int J Hydrogen Energy 2020;45: 2308–18. https://doi.org/10.1016/j.ijhydene.2019.11.092.

[32] Apostolou D, Enevoldsen P, Xydis G. Supporting green Urban mobility – the case of a small-scale autonomous hydrogen refuelling station. Int J Hydrogen Energy 2019;44:9675–89. https://doi.org/10.1016/j.ijhydene.2018.11.197.

[33] Reddi K, Elgowainy A, Rustagi N, Gupta E. Impact of hydrogen refueling configurations and market parameters on the refueling cost of hydrogen. Int J Hydrogen Energy 2017;42:21855–65. https://doi.org/10.1016/j. ijhydene.2017.05.122.

[34] Kawatsu K, Suzuki T, Shiota K, Izato Y ichiro, Komori M, Sato K, et al. Trade-off study between risk and benefit in safety devices for hydrogen refueling stations using a dynamic physical model. Int J Hydrogen Energy 2022;47:24242–53. https://doi.org/10.1016/j.ijhydene.2022.05.028.

[35] Perna A, Minutillo M, Di Micco S, Jannelli E. Design and costs analysis of hydrogen refuelling stations based on different hydrogen sources and plant configurations. Energies 2022;15. https://doi.org/10.3390/en15020541.

[36] Grüger F, Dylewski L, Robinius M, Stolten D. Carsharing with fuel cell vehicles: sizing hydrogen refueling stations based on refueling behavior. Appl Energy 2018; 228:1540–9. https://doi.org/10.1016/j.apenergy.2018.07.014.

[37] Grüger F, Hoch O, Hartmann J, Robinius M, Stolten D. Optimized electrolyzer operation: employing forecasts of wind energy availability, hydrogen demand, and electricity prices. Int J Hydrogen Energy 2019:4387–97. https://doi.org/10.1016/j.ijhydene.2018.07.165.

[38] Maurer W, Rechberger P, Justl M, Keuschnigg R. Parameter study for dimensioning of a PV optimized hydrogen supply plant. Int J Hydrogen Energy 2022;47: 40815–25. https://doi.org/10.1016/j.ijhydene.2022.09.183.

[39] Böhm H, Goers S, Zauner A. Estimating future costs of power-to-gas – a component-based approach for technological learning. Int J Hydrogen Energy 2019;44: 30789–805. https://doi.org/10.1016/j.ijhydene.2019.09.230.

[40] Mariani A, Prati MV, Unich A, Morrone B. Combustion analysis of a spark ignition i. c. engine fuelled alternatively with natural gas and hydrogen-natural gas blends. Int J Hydrogen Energy 2013;38:1616–23. https://doi.org/10.1016/j.ijhydene.2012.11.051.

[41] Zhang Y, Gao W, Yu Y, Wang M, Chen C. Primary air ratio change and gas interchangeability index correct for domestic gas cooker burning multi-source natural gases. J Nat Gas Sci Eng 2016;35:276–82. https://doi.org/10.1016/j.jngse.2016.08.060.

[42] Choudhury S, McDonell VG, Samuelsen S. Combustion performance of low-NOx and conventional storage water heaters operated on hydrogen enriched natural gas. Int J Hydrogen Energy 2020;45:2405–17. https://doi.org/10.1016/j.ijhydene.2019.11.043.

[43] Lo Basso G, Pastore LM, Sgaramella A, Mojtahed A, de Santoli L. Recent progresses in H2NG blends use downstream Power-to-Gas policies application: an overview over the last decade. Int J Hydrogen Energy 2023. https://doi.org/10.1016/j.ijhydene.2023.06.141.

[44] Qiu Y, Zhou S, Gu W, Lu Y, Zhang XP, Zhang K, et al. Network modeling and operation optimization of electricity-HCNG-integrated energy system. CSEE Journal of Power and Energy Systems 2023;9:1251–65. https://doi.org/10.17775/CSEEJPES.2022.07810.

[45] Khab H, Chaker A, Ziani L. Effects of pressure and hydrogen addition to methane on the temperatures within a pressurized cylinder during the vehicle refueling of HCNG. Int J Hydrogen Energy 2019;44:22437–44. https://doi.org/10.1016/j.ijhydene.2019.04.209.

[46] Sgaramella A, Lo Basso G, de Santoli L. How the cylinder initial conditions affect the HCNG refuelling process - a thermodynamic analysis to determine the most effective filling parameters. Int J Hydrogen Energy 2023. https://doi.org/10.1016/j.ijhydene.2023.07.323.

[47] Zareei J, Rohani A. Optimization and study of performance parameters in an engine fueled with hydrogen. Int J Hydrogen Energy 2020;45:322–36. https://doi.org/10.1016/j.ijhydene.2019.10.250.

[48] PVGIS Online Tool. Https://[Joint-Research-CentreEcEuropaEu/Pvgis-Online-Tool_en n.d].

[49] White CM, Steeper RR, Lutz AE. The hydrogen-fueled internal combustion engine: a technical review. Int J Hydrogen Energy 2006;31:1292–305. https://doi.org/10.1016/j.ijhydene.2005.12.001.

[50] Chintala V, Subramanian KA. Hydrogen energy share improvement along with NOx (oxides of nitrogen) emission reduction in a hydrogen dual-fuel compression ignition engine using water injection. Energy Convers Manag 2014;83:249–59. https://doi.org/10.1016/j.enconman.2014.03.075.

[51] H2A hydrogen delivery infrastructure analysis models and conventional pathway options analysis results. 2008.

[52] Mayer T, Semmel M, Guerrero Morales MA, Schmidt KM, Bauer A, Wind J. Techno-economic evaluation of hydrogen refueling stations with liquid or gaseous stored hydrogen. Int J Hydrogen Energy 2019;44:25809–33. https://doi.org/10.1016/j.ijhydene.2019.08.051.

[53] Zheng J, Ye J, Yang J, Tang P, Zhao L, Kern M. An optimized control method for a high utilization ratio and fast filling speed in hydrogen refueling stations. Int J Hydrogen Energy 2010;35:3011–7. https://doi.org/10.1016/j.ijhydene.2009.07.001.

[54] Kurtz J, Bradley T, Winkler E, Gearhart C. Predicting demand for hydrogen station fueling. Int J Hydrogen Energy 2020;45:32298–310. https://doi.org/10.1016/j.ijhydene.2019.10.014.

[55] Lo Basso G, Pastore LM, Mojtahed A, de Santoli L. From landfill to hydrogen: techno-economic analysis of hybridized hydrogen production systems integrating biogas reforming and Power-to-Gas technologies. Int J Hydrogen Energy 2023. https://doi.org/10.1016/j.ijhydene.2023.07.130.

[56] Ferrari ML, Rivarolo M, Massardo AF. Hydrogen production system from photovoltaic panels: experimental characterization and size optimization. Energy Convers Manag 2016;116:194–202. https://doi.org/10.1016/j.enconman.2016.02.081.

[57] Phan Van L, Hieu Hoang L, Nguyen Duc T. A comprehensive review of direct coupled photovoltaic-electrolyser system: sizing techniques, operating strategies, research progress, current challenges, and future recommendations. Int J Hydrogen Energy 2023. https://doi.org/10.1016/j.ijhydene.2023.03.257.

[58] de Groot MT, Kraakman J, Garcia Barros RL. Optimal operating parameters for advanced alkaline water electrolysis. Int J Hydrogen Energy 2022;47:34773–83. https://doi.org/10.1016/j.ijhydene.2022.08.075.

[59] Amireh SF, Heineman NN, Vermeulen P, Barros RLG, Yang D, van der Schaaf J, et al. Impact of power supply fluctuation and part load operation on the efficiency of alkaline water electrolysis. J Power Sources 2023;560. https://doi.org/10.1016/j.jpowsour.2023.232629.

[60] Ursúa A, Gandía LM, Sanchis P. Hydrogen production from water electrolysis: current status and future trends. In: Proceedings of the IEEE, 100. Institute of Electrical and Electronics Engineers Inc.; 2012. p. 410–26. https://doi.org/10.1109/JPROC.2011.2156750.

[61] Haug P, Koj M, Turek T. Influence of process conditions on gas purity in alkaline water electrolysis. Int J Hydrogen Energy 2017;42:9406–18. https://doi.org/10.1016/j.ijhydene.2016.12.111.

[62] Thomas CE, Reardon JP, Lomax FD, Pinyan J, Kuhn IF. Distributed hydrogen fueling systems analysis. n.d.

[63] Marciuš D, Kovač A, Firak M. Electrochemical hydrogen compressor: recent progress and challenges. Int J Hydrogen Energy 2022;47:24179–93. https://doi.org/10.1016/j.ijhydene.2022.04.134.

[64] Niazmand A, Farzaneh-Gord M, Deymi-Dashtebayaz M. Exergy analysis and entropy generation of a reciprocating compressor applied in CNG stations carried out on the basis models of ideal and real gas. Appl Therm Eng 2017;124:1279–91. https://doi.org/10.1016/j.applthermaleng.2017.06.035.

[65] Perry's chemical engineers' handbook physical and chemical data conversion factors and mathematical symbols contents. 1999.

[66] Li CH, Zhu XJ, Cao GY, Sui S, Hu MR. Dynamic modeling and sizing optimization of stand-alone photovoltaic power systems using hybrid energy storage technology. Renew Energy 2009;34:815–26. https://doi.org/10.1016/j.renene.2008.04.018.

[67] James Larminie, Andrew Dicks. Fuel cell systems explained. J. Wiley; 2003.

[68] Petrollese M, Concas G, Lonis F, Cocco D. Techno-economic assessment of green hydrogen valley providing multiple end-users. Int J Hydrogen Energy 2022;47: 24121–35. https://doi.org/10.1016/j.ijhydene.2022.04.210.

[69] Fan JL, Yu P, Li K, Xu M, Zhang X. A levelized cost of hydrogen (LCOH) comparison of coal-to-hydrogen with CCS and water electrolysis powered by renewable energy in China. Energy 2022;242. https://doi.org/10.1016/j.energy.2021.123003.

[70] Lo Basso G, Mojtahed A, Pastore LM, De Santoli L. High-temperature green hydrogen production: a innovative– application of SOEC coupled with AEC through sCO2 HP. Int J Hydrogen Energy 2023. https://doi.org/10.1016/j.ijhydene.2023.04.231.

[71] USDrive. Hydrogen storage technologies Roadmap hydrogen delivery technical team Roadmap. 2013.

[72] Parks G, Boyd R, Cornish J, Remick R, Review Panel I. Hydrogen station compression, storage, and dispensing technical status and costs. Syst Integrat 2020.

[73] Turton R, Bailie RC, Whiting WB, Shaeiwitz JA, Bhattacharyya D. Analysis, synthesis, and design of chemical processes fourth edition. n.d.

[74] Ferrero D, Gamba M, Lanzini A, Santarelli M. Power-to-Gas hydrogen: techno-economic assessment of processes towards a multi-purpose energy carrier. In: Energy procedia, 101. Elsevier Ltd; 2016. p. 50–7. https://doi.org/10.1016/j.egypro.2016.11.007.

[75] Renewable Energy Agency I. Renewable power generation costs in 2019. 2020.

[76] Pierro M, Perez R, Perez M, Prina MG, Moser D, Cornaro C. Italian protocol for massive solar integration: from solar imbalance regulation to firm 24/365 solar generation. Renew Energy 2021;169:425–36. https://doi.org/10.1016/j.renene.2021.01.023.

[77] De Santoli L, Lo Basso G, Bruschi D. A small scale H2NG production plant in Italy: techno-economic feasibility analysis and costs associated with carbon avoidance. Int J Hydrogen Energy 2014;39:6497–517. https://doi.org/10.1016/j.ijhydene.2014.02.003.

[78] Schneider J, Meadows G, Mathison SR, Veenstra MJ, Shim J, Immel R, et al. Validation and sensitivity studies for SAE J2601, the light duty vehicle hydrogen fueling standard. SAE International Journal of Alternative Powertrains 2014;3: 257–309. https://doi.org/10.4271/2014-01-1990.

[79] Reddi K, Elgowainy A, Rustagi N, Gupta E. Impact of hydrogen SAE J2601 fueling methods on fueling time of light-duty fuel cell electric vehicles. n.d.

[80] James W. An introduction to SAE hydrogen fueling standardization. 2014.

[81] Energy Commission C. California Energy Commission California Air Resources Board Joint Agency Staff Report on Assembly Bill 8: 2021 Annual assessment of time and cost needed to attain 100 hydrogen refueling stations in California. n.d.

[82] Solar Costs n.d. https://www.irena.org/Statistics/View-Data-by-Topic/Costs/Solar-Costs (accessed February 18, 2022).

[83] ACEA acqua. Tariffe per la fornitura. Https://WwwGruppoAceaIt/al-Servizio-Delle-Persone/Acqua/Acea-Ato-2/Tariffe-per-La-Fornitura n.d.

[84] ARERA. Dati statistici. Https://WwwAreraIt/It/Dati/Elenco_datiHtm n.d.

[85] GME- Gestore Mercati Energetici. Esiti Mercato Elettrico. Https://WwwMercatoelettricoOrg/It/n.d.

[86] ICE Endex. Dutch TTF Natural Gas Futures. Https://WwwTheiceCom/Products/27996665/Dutch-TTF-Gas-Futures/Data?MarketId=5544919 n.d.

[87] Pastore LM, Lo Basso G, de Santoli L. Can the renewable energy share increase in electricity and gas grids takes out the competitiveness of gas-driven CHP plants for distributed generation? Energy 2022;256. https://doi.org/10.1016/j.energy.2022.124659.

[88] Tabella parametri standard nazionali. [n.d].

[89] ISPRA. indicatori di efficienza e decarbonizzazione del sistema energetico nazionale e del settore elettrico n.d.

[90] ISPRA. Fattori di emissione atmosferica di gas a effetto serra nel settore elettrico nazionale e nei principali Paesi Europei n.d.

[91] Alirahmi SM, Assareh E, Arabkoohsar A, Yu H, Hosseini SM, Wang X. Development and multi-criteria optimization of a solar thermal power plant integrated with PEM electrolyzer and thermoelectric generator. Int J Hydrogen Energy 2022;47: 23919–34. https://doi.org/10.1016/j.ijhydene.2022.05.196.

[92] Cabrera P, Carta JA, Lund H, Thellufsen JZ. Large-scale optimal integration of wind and solar photovoltaic power in water-energy systems on islands. Energy Convers Manag 2021;235:113982. https://doi.org/10.1016/J.ENCONMAN.2021.113982.

[93] Dorotić H, Pukšec T, Duić N. Economical, environmental and exergetic multi-objective optimization of district heating systems on hourly level for a whole year. Appl Energy 2019;251:113394. https://doi.org/10.1016/J. APENERGY.2019.113394.

[94] Liu H, Li Y, Duan Z, Chen C. A review on multi-objective optimization framework in wind energy forecasting techniques and applications. Energy Convers Manag 2020;224:113324. https://doi.org/10.1016/J.ENCONMAN.2020.113324.

[95] Mangkuto RA, Rohmah M, Asri AD. Design optimisation for window size, orientation, and wall reflectance with regard to various daylight metrics and lighting energy demand: a case study of buildings in the tropics. Appl Energy 2016; 164:211–9. https://doi.org/10.1016/J.APENERGY.2015.11.046.

[96] Phan-Van L, Dinh VN, Felici R, Duc TN. New models for feasibility assessment and electrolyser optimal sizing of hydrogen production from dedicated wind farms and solar photovoltaic farms, and case studies for Scotland and Vietnam. Energy Convers Manag 2023;295:117597. https://doi.org/10.1016/j. enconman.2023.117597.